

# Comparative Analysis of Different Convergent Section Angles and Working Fluids on Supersonic Nozzle Thrust Force by Computational Fluid Dynamic (CFD)

R. Chohan<sup>1</sup>, I. M. Chohan<sup>2</sup>, M. Chohan<sup>3</sup>

<sup>1</sup>Institute of Computer Science, Shah Abdul Latif University (SALU), Khairpur Mir's, Sindh, Pakistan

<sup>2</sup>Department of Mechanical Engineering, Universiti Teknologi Petronas (UTP), Seri Iskandar 32610, Malaysia

<sup>3</sup>Department of Computer Science, Begum Nusrat Bhutto Women University, Sukkur, Sindh, Pakistan

<sup>1</sup>[Rozina.chohan@salu.edu.pk](mailto:Rozina.chohan@salu.edu.pk)

**Abstract-** Nozzles are the important part of propellers generating the thrust and enabling the rockets to move in a forward direction. However, their efficient design is imperative to enhance the thrust force and to reduce fuel consumption. Therefore, the aim of this study is to conduct a comparative study of different convergent section angles to evaluate the maximum thrust force of a supersonic nozzle. Computational fluid dynamic (CFD) simulation is performed with different convergent section angles ranging from 42° to 24° by maintaining the same pressure ratio and operating conditions. In addition, the numerical simulation is performed with different working fluids such as air, carbon dioxide, and carbon monoxide. Furthermore, the effect of inlet temperature on Mach number is also analysed. The numerical simulation is performed on an unstructured grid. Meanwhile, the simulation is carried out on a 2D axisymmetric density-based coupled solver with a viscous k-Omega SST turbulence model. The results are validated with previous experimental work and found good agreement with 2.6 percent error. The study revealed that decreasing the convergent angle up to 27° has a favourable effect, and a 1.6 percent increase in thrust force was estimated. Additionally, CO<sub>2</sub> was considered the best working gas with the highest thrust performance, preceded by air, nitrogen, and CO. Furthermore, the inlet temperature has a significant effect on the nozzle Mach number. The findings of this study may be used to design efficient jet engines and rockets.

**Keywords-** Supersonic Nozzle, Convergent Divergent Nozzle, Computational Fluid Dynamics.

## I. INTRODUCTION

Since Aircrafts rely on non-renewable, polluting, and depleting fossil fuels, and fuel consumption accounts for approximately 20% of

airline operational costs [1]. Therefore, its energy efficient design is necessary to achieve the global environmental and energy requirements. Propulsion system efficiency is highly influenced by the nozzle performance, which is a critical component responsible for the generation of power for aircraft [2]. The nozzle is designed to control the velocity, temperature, and pressure of a fluid. Additionally, it transforms thermal energy into the kinetic energy. The fluid with high temperature and pressure, that enter the nozzle escape with high velocity and low pressure. The nozzle's primary function is to release gases at extremely high velocities while simultaneously lowering the pressure to an extremely low level. As a result, there is increased backward momentum, allowing heavier aircraft to fly in air due to thrust force [3-4]. Airplanes, space shuttles, Ramjets, scramjets, and rocket engines commonly use nozzles with a fixed convergent part followed by a fixed diverging section [5-6]. Numerous studies have been done to find the nozzle geometry effect on its performance [7-9]. The findings of those investigations led to the innovation of a convergent nozzle with a divergent portion, that made it possible to get supersonic exhaust. Furthermore, Bayt, R.L and Khatab N [10-11] found that an increment in the volume of the divergent portion has direct proportionality with the velocity of the flue gas, that leads to drop the density of the gas because of its speed at the supersonic range. Balabel, A., found that average fluid velocity field, pressure and turbulent characteristics have an impact on a verity of physical process occurring inside the nozzle [12]. Supersonic nozzles provide thrust force in propulsion systems [13]. Furthermore, Grissik [14] investigated the losses inside the nozzle and discovered three key elements such as viscus losses, kinetic losses, and divergence losses that increase the overall losses inside the nozzle. Furthermore, their investigation indicated that modifications to the nozzle divergence part have a substantial impact on

viscous losses. Additionally, it was discovered that decreasing the divergence angle from  $45^\circ$  to  $20^\circ$  has another favourable impact by lowering chemical kinetic losses. In 2005 A.D [15] discovered that the length of the nozzle had a substantial effect on the exit flow velocity; reducing the length of the nozzle enhanced the exit flow velocity. In addition, it was found that increasing the divergence angle from  $20^\circ$  to  $40^\circ$  with minimal viscous effects can improve the impulse force. These computational results confirm the experimental findings of Whalen [16], who discovered that a conical nozzle with a divergence angle of  $25^\circ$  performs better than one with a divergence angle of  $20^\circ$ . Noh [17], studied the effect of the divergent portion of the nozzle on the thrust coefficient. The findings revealed that decreasing the divergent angle from  $28^\circ$  to  $24^\circ$  had a negative effect, accounting for an 18% decrease in thrust force, while increasing the divergent angle from  $16^\circ$  to  $18^\circ$  increased the thrust coefficient. Moreover, it was shown that flow separation at the walls of diverging portions can be controlled but not eliminated. Kim [18] conducted CFD simulation of a miniature nozzle having a through-diameter less than 1 mm and discovered that the discharge coefficient is highly influenced by the diffuser angle. In 2022, Hekun Lia [19] investigated the effect of nozzle design on fuel efficiency and emission. Their study found an improvement in the Trade-off between NOx emission and fuel consumption obtained from elliptic nozzle at four different forces. Moreover, Zhipeng [20] in 2023 investigated the effect of atmospheric pressure and number of nozzle on fuel efficiency and shoot emissions. They found at high altitude like 3000 meters the nozzle fuel efficiency reduced, and the optimal number were approximately six that provided best results at all altitudes.

From extensive literature, it was found that numerous studies have been conducted to analyse the effect of different parts (length, outlet diameter, inlet diameter, throat, and divergent section angle) of the CD nozzle on its performance, but less attention is given to the convergent section angle. Additionally, in previous literature, most of the studies assumed air as the working fluid. However, in actual conditions, after the combustion of fuel, different gases exhaust from the nozzle. Therefore, this paper focused on overcoming that gap and presents the effect of the nozzle convergent angle as well as the different working fluids (CO<sub>2</sub>, CO, and air) on the thrust force to make a fair comparison and to obtain the best inlet design with maximum performance.

### 1.1. Additional Literature on Turbulence Modelling

The CFD simulation of compressible turbulent flows remains a difficult problem for engineers and scientists. Recently, numerous studies have been done to simulate and comprehend the flow

behaviour inside supersonic rocket nozzles. Nozzle simulation has gained immense importance due to their numerous applications. The flow development within the rocket burning solid is critical in the design and optimization of the rocket's nozzle [21]. The goal of any supersonic nozzle design should be improved thrust performance, and CFD analysis is the most accurate and efficient way to predict and determine the thrust coefficient [22]. However, the precision of CFD simulation is crucial for providing trustworthy, accurate, and reliable outcomes [23-24]. There are variety of computational models range from the simplest algebraic, non-linear, and linear to extremely complicated two equation models. Selecting the appropriate turbulence model is also crucial for achieving reliable computational fluid dynamics (CFD) results when dealing with complex fluid flow issues [25]. In that context, El-Askary, W., and A. Balabel [26] investigated the efficacy of numerous turbulence models to analyse complex fluid flow and found that the selection of an appropriate model was dependent on the mechanism of problems such as turbulence, temperature, pressure, and highly viscous fluids. A two-equation turbulence model was also found to be more trustworthy for separated and viscous flows. Now a days, the Reynolds stress model and the non-linear eddy viscosity model are the gold standards for turbulence modelling. While the Eddy viscosity model is well-suited to modelling re-attaching turbulent flows, its solution instability at large time steps is a major drawback [27]. Currently, RANS equations have been proven to be the most viable in the case of separated and viscous flows when combined with a near-wall function to modify turbulent viscosity around the solid walls [28]. Even though modelling flow simulation solely with the RANS model cannot produce precise results that can be verified with experimental data, once have need to find that best turbulence model to get fair result so that could be verified with experimental work [29-30]. To resolve this issue number of studies were conducted to find out best turbulence model for supersonic flow simulation such as JP Dussauge et.al and KJ Plotkin [31-32] conducted the study and observed that the location of shock waves and the degree of separation were found to be two of the most significant factors influencing flow turbulence. Therefore, it was difficult to recommend a single model for turbulence modelling that will reliably and accurately predict turbulence. However, a study that analysed the efficiency of various turbulence models to experimental results discovered that the K-omega model has a high correlation with experimental data [33]. Though the k-omega is better, but it creates problem in the case of shear flow due to sensitivity of omega value [34]. However, this issue was resolved by Menter's K-omega SST model that associates the benefits of both k-omega and k-epsilon model for the study of

near and away wall flow [35]. Considering those benefits, k-omega SST model is used in this research for the simulation of CD nozzle.

## II. METHODOLOGY

### 2.1. Nozzle Computational Modelling and Meshing

The design parameters and boundary conditions/operating conditions of CD nozzle were taken from reference [36], shown in Table 1, Table 2 and Fig 1. Those parameters considered as baseline parameters of nozzle then angle of convergent section was decreased from 42° to 24° with the gape of 3° in every case.

Since the nozzle design was symmetry, 2D axis-symmetry model was developed on ANSYS design modeler to save computational time. The grids were generated using ANSYS ICEM. The hybrid meshing was employed to enhance the quality of mesh. The quality of the mesh further improved using mesh refinement and inflation to improve solution accuracy. Inflation technique was applied near the wall of divergent section to clearly obtain the flow separation and boundary layer effects shown in Fig 2. Further grid information is presented in Table 3.

Table 1: Design Parameters of Supersonic Nozzle

Sr. No	Parameters	Specifications
1	Inlet Diameter	20mm
2	Outlet Diameter	20mm
3	Throat Radius	2mm
4	Convergent Angle	42°
5	Throat Diameter	7mm
6	Divergent Angle	32°

Table 2: Boundary Conditions of Supersonic Nozzle

Sr. No	Factors	Value
1	Inlet Pressure	500000 (Pa)
2	Pressure ambient	101325 (Pa)
3	Temperature ambient	300 (K)

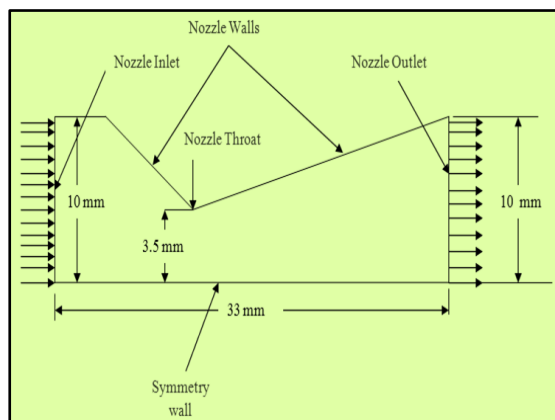


Figure 1: Nozzle 2D axisymmetric Geometry

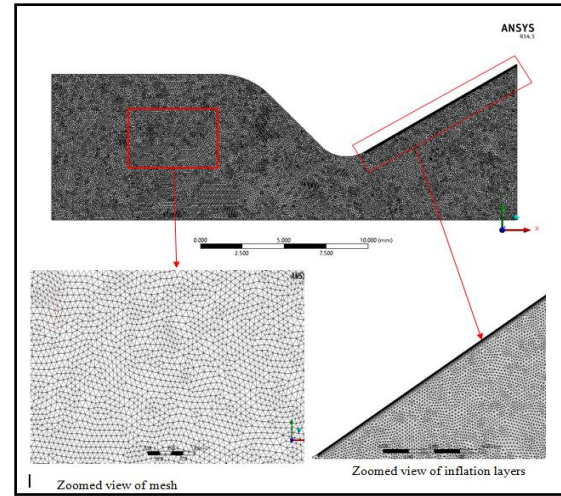


Figure 2: Grid of 2D Nozzle Model

Table 3: Grid Information of Domain

Domain	Fluid
Element Type	Hybrid (Triangular and rectangular)
Grid Quality (Orthogonal)	0.80
Number of Nodes	124977
Number of Elements	902489

### 2.2. Governing Equations

The basic conservation principals of energy, mass, and momentum are used to derive the governing equations for fluid flow, including the momentum equation, energy equation, and continuity equation. Due to the chaotic changes in fluid properties, those equations are Partial Differential Equations (PDE), which are notoriously challenging to solve analytically or numerically. Thus, by employing Reynolds averaging, these intricate equations are simplified. The typical fluid velocity along the X-axis is defined in Equation (1)

$$u_i = \bar{u}_i + u'_i \quad (1)$$

Where,  $\bar{u}_i$  and  $u'_i$  are the average and fluctuating components and  $u_i$  is the velocity.

Similarly, density can be decomposed in average and fluctuating components as expressed in Equation (2)

$$\rho = \bar{\rho}_i + \rho'_i \quad (2)$$

Where,  $\bar{\rho}_i$  is the mean component of density  $i$ ,  $\rho'_i$  fluctuation component of density  $i$ .

The time average components can be obtained using Reynolds average technique as defined in Equation (3).

$$\frac{\partial \rho}{\partial t} + \frac{\partial}{\partial x_i} (\rho u_i) = 0 \quad (3)$$

$$\frac{\partial}{\partial t} (\rho u_i) + \frac{\partial}{\partial x_j} (\rho u_i u_j) = \frac{\partial p}{\partial x_i} +$$

$$\frac{\partial}{\partial x_j} \left[ \mu \left( \frac{\partial u_i}{\partial x_j} + \frac{\partial u_j}{\partial x_i} \right) \right] + \frac{\partial}{\partial x_j} (-\rho \bar{u}'_i \bar{u}'_j) \quad (4)$$

Where,  $\rho$ ,  $\mu$ ,  $\delta_{ij}$ ,  $\rho \tilde{u}_i \tilde{u}_j'$ , and  $x_i, x_j$  are the pressure, dynamic viscosity, Kronecker delta, Reynolds stress tensors, and special coordinates, respectively.

The Reynold stresses are modelled by selecting K-omega shear stress transport model commonly referred as K-omega SST model due to its combined benefits as mentioned at section 1.2. The transport equations of K-Omega SST model are written below in Equation (5) and Equation (6).

$$\frac{\partial(\rho k)}{\partial t} + \frac{\partial(\rho k u_i)}{\partial x_i} = \frac{\partial}{\partial x_j} \left( \Gamma k \frac{\partial k}{\partial x_j} \right) + \tilde{G}_k - Y_k + S_k \quad (5)$$

$$\frac{\partial(\rho \omega)}{\partial t} + \frac{\partial(\rho \omega u_i)}{\partial x_i} = \frac{\partial}{\partial x_j} \left( \Gamma \omega \frac{\partial \omega}{\partial x_j} \right) + \tilde{G}_\omega - Y_\omega + D_\omega + S_\omega \quad (6)$$

Where,  $\Gamma k$  and  $\Gamma \omega$  are diffusivity,  $\tilde{G}_k$  and  $\tilde{G}_\omega$  are turbulent kinetic energy and dissipation,  $Y_k$  and  $Y_\omega$  are dissipation terms, and  $D_\omega$  are cross diffusion terms, respectively.

### 2.3. Grid Generation

As the quality of the grid has a substantial effect on the accuracy of the numerical solution, it was essential to improve it in the zone of high-pressure gradient to achieve accurate results at a low computing cost. The entire computational area was initially coarsely meshed with cells and faces. Second, cells were chosen for further refinement based on user-defined criteria or Richardson-extrapolation. This procedure smoothed out all the rough edges and leaved only the finest cells. Once the mesh was adapted, the integrator forwards the time for individual mesh cells that was at the same refined level. A correction procedure was utilised to move the conserved parameters between the interfaces of coarse and fine grid cells to guarantee that the values leaving one grid cell precisely match the values entering at the other cell borders. If the degree of refinement in the flow domain ever reaches its lowest value, the highly refined grid may also be withdrawn or substituted with a coarser grid.

### 2.3. Numerical Scheme

Setting the numerical scheme and selecting the turbulence model were critical steps to avoid errors and produce more precise results from computer model. Consequently, a second-order upwind discretization strategy was used in this study to determine the equation's solutions as shown in Fig 3.

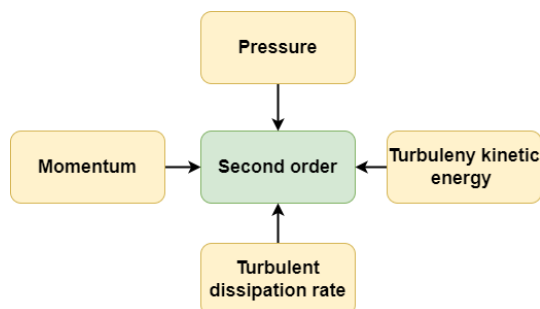


Figure 3: Discretising Schemes Used for Equations

The value of the eastern face is predicted by two upwind nodes. It was assumed that the gradient between the considered node and the eastern face is equal as the gradient between the considered node and the western node (see Equation (7)).

$$\frac{\phi_e - \phi_p}{x_e - x_p} = \frac{\phi_p - \phi_w}{x_p - x_w} \Rightarrow \phi_e = \frac{(\phi_p - \phi_w)(x_e - x_p)}{x_p - x_w} + \phi_p \quad (7)$$

Where,  $e, p, w$ , and  $w$  are the east face, present cell, west cell, and location in respective direction, respectively. While  $\phi$  is scalar quantity like temperature and velocity.

For more precision, a multidimensional linear reconstruction method was utilised to compute the number of cells faces. This technique leverages the Taylor expansion series for cell-centered solutions about the cell-centroid to achieve higher order precision. Consequently, when the second-order upwind discretization scheme was selected, the values of were calculated using the following Equation (8)[37].

$$\phi_f = \phi + \nabla \phi \cdot \Delta \vec{S} \quad (8)$$

Where,  $\phi_f$  is interpolation face value.  $\nabla \phi$  and  $\Delta \vec{S}$  are gradient of scalar variables and face factors.

### 2.5. FMG Initialization

Once the case was started, the text user interface command of the FMG initialization can be used to further enhance the numerical solution. In essence, FMG was utilised to speed up the simulation's convergence rate. The computing time was shortened by two ways. The first technique assumes that the flow is inviscid, which minimises the quantity of flow controlling equations and thus shortens computing time. According to the numerical simulations, the computing time for viscous flows was cut in half by considering flow inviscid. In the second instance. Since one tetrahedron is formed when five tetrahedral cells are combined in three-dimensional grids, computation time is reduced by a factor of five times. The full multi-grid initialization method can be seen in Fig 4. Additionally, it was discovered that the solution initialised by FMG was much closer to the final solution initialised by the general initialization approach.

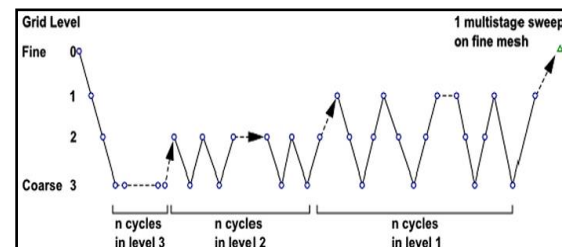


Figure 4: FMG initialization method [38]

### 2.6. Nozzle Thrust Force

Thrust is the working fluid's acceleration's reaction force and the force caused by a propellant's momentum change. Newton's third law produces

thrust (For every action there is an equal and opposite reaction). It drives the rocket through the air and space. Rocket motors produce it. When propellant is expelled from the nozzle in one direction, thrust is generated in the opposite direction. Rocket thrust depends on exhaust velocity, propellant mass flow rate, and nozzle exit pressure. The general thrust force can be obtained by using Equation (9).

$$T = \dot{m}_e V_e - \dot{m}_{in} V_{in} + (p_e - p_a) * A_e \quad (9)$$

Whereas,

$T$  represents the thrust nozzle thrust force.

$\dot{m}_{in}$ = mass flow rate at inlet

$\dot{m}_e$ = mass flow rate at outlet

$V_{in}$ = inlet velocity

$V_e$ = outlet velocity

$p_e$ = outlet pressure

$p_a$ = ambient pressure

$A_e$ = exit area

### 2.7. Validation

Linares [36] conducted the experimental work to find out the nozzle thrust force. They put nozzle at vertical direction, maintained the nozzle inlet pressure using compressed air in cylinder. Whereas the thrust force was measured using load cells at the outlet of nozzle. The current CFD result is validated with that data and presented in Table 4. The computational model result has good agreement with experimental result with just 2.16 percent of error. The nozzle walls were assumed by the CFD simulation to be adiabatic (no heat loss), but, during experimental work, the nozzle wall may lose heat, which could be the cause of that error. After validation of CFD model, the convergent section angle was changed keeping other design parameters same so that its effect may be analysed.

Table 4. CFD Model Validation

Baseline design	42
Experimental Work [36]	22.65
Computational fluid dynamic Simulation results	23.139
Error	2.16

## III. RESULTS AND DISCUSSION

The pressure contour plot against nozzle angles is shown for three convergent angles, including 24°, 33°, and 42°, in Fig 6(a), Fig 6(b), and Fig 6(c), respectively. From these plots, it was determined that the pressure is highest at the nozzle inlet, decreases down along the length of the nozzle, and finally reaches its lowest point at the nozzle outlet. Furthermore, the results of the pressure plot showed that the pressure is nearly constant in the settling chamber section and drops off sharply in the convergent section. It was also determined via pressure contour plot that the nozzle convergent

section angle has a major impact on the pressure.

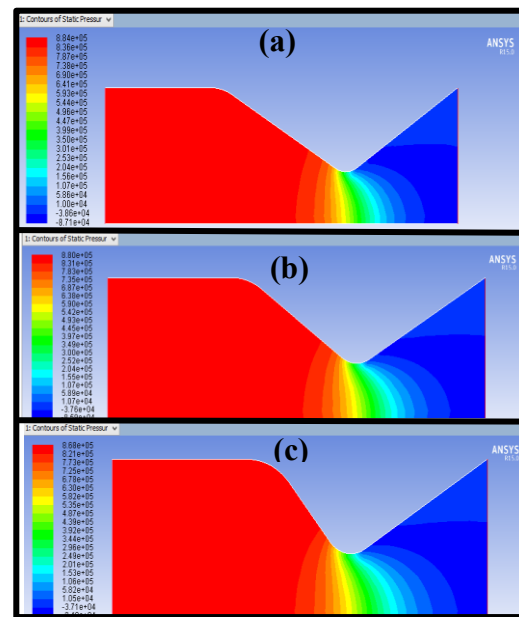


Figure 6: Pressure Contour Plots (a) 27° convergent angle, (b) 33° convergent angle, and (c) 42° convergent angle.

Fig 7 (a), Fig 7(b), and Fig 7(c) shows the velocity contour plots with convergent angle 24°, 33°, and 42°, respectively. From these figures it was observed that velocity variation is highly nonlinear throughout the nozzle, except for the settling chamber. Through velocity contour, it was determined that the fluid velocity at the nozzle inlet is nearly zero. Variation of velocity inside a supersonic nozzle revealed that velocity increases along the length and reaches the speed of sound at the throat, while velocity increment continued in the divergent portion of the nozzle.

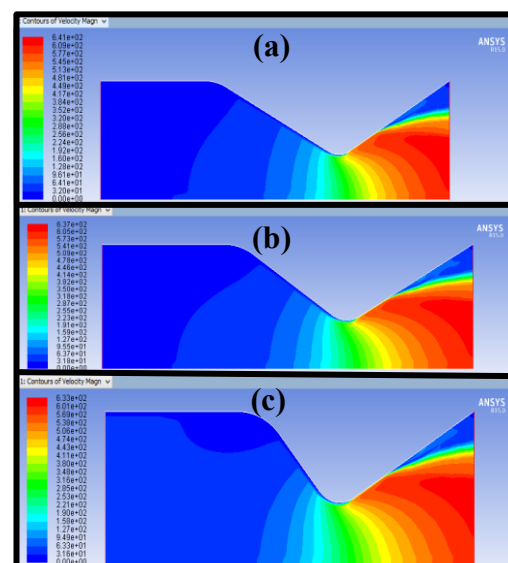


Figure 7: Velocity Contour Plots (a) 27° convergent angle, (b) 33° convergent angle, and (c) 42° convergent angle.

### 3.2. Thrust Force with Respect to Convergent Angles

The thrust force was determined for seven nozzle models by using Equation 9, and the results are shown in Table 6 and Fig 8. It was observed that out of the seven nozzles tested, the one with convergent section angle of 42° (baseline) produced the lowest thrust force of 23.139 newton and found that by decreasing the nozzle's convergent angle up to 27-degree resulting increase in thrust force up to 23.50 newton but going below that angle has no beneficial effect on thrust force. In addition, a 1.6% enhancement of thrust force was found at 27-degree of convergent angle compared to its original design.

Table 6: Thrust Force of Nozzles

Angle (Degree)	Velocity (Outlet)	Pressure (Outlet)	Mass Flow Rate (m/s)	Thrust Force (Newton)
42	616	-60932	0.12	23.139
39	618	-61244	0.12	23.20
36	621	-62265	0.12	23.30
33	620	-61747	0.12	23.38
30	622	-62293	0.12	23.45
27	624	-62833	0.12	23.50
24	623	-63250	0.12	23.25

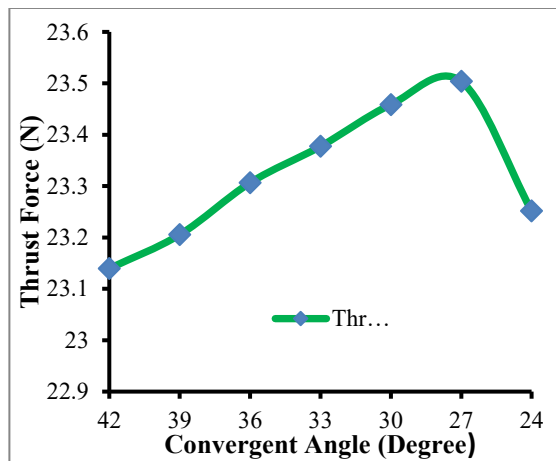


Figure 8: Supersonic Nozzle Thrust Force

### 3.3. Thrust Force with Respect to Different Fluids

Working fluid characteristics like density, viscosity, thermal conductivity, and specific heat capacity all have a significant impact on nozzle thrust. When four different working fluids, such as air, nitrogen, carbon monoxide (CO), and carbon dioxide (CO<sub>2</sub>), are allowed to flow through a nozzle under the operating conditions, thrust force is produced as shown in Fig 9. These working fluids were chosen because they are important combustion process by-products. In addition, air is chosen as a working fluid because it is easily available and expenses almost nothing, making it a popular choice among researchers. Thrust forces are plotted against working fluids in Fig 9. According to Fig 9, the maximum thrust is produced when CO<sub>2</sub> is used as

the working fluid, followed by Nitrogen, air, and CO. Therefore, it can be said that combustion with the highest production of CO<sub>2</sub> and the least amount of CO is more advantageous for both the environment and thrust generation.

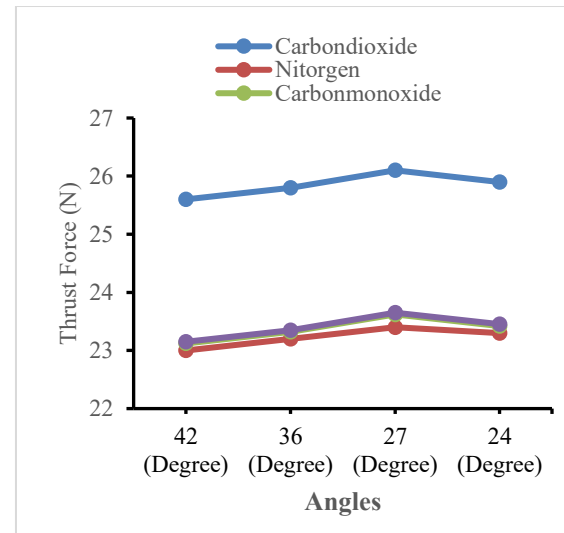


Figure 9: Thrust Force with Respect to Angles and Working Fluids

### 3.4. Effect of Inlet Temperature

The effect of inlet temperature on Mach number have also been analysed in this paper because increase in Mach number Cause increase in thrust force. Since the settling chamber has a constant cross-sectional area and because the Mach number or fluid velocity is typically very low at the nozzle inlet, it can be seen from the Mach number variation graph along the length of the nozzle that variation is very low there. After the settling chamber, a sharp increase in Mach was seen from the convergent section to the nozzle's exit. It is deduced from Fig 10, that the Mach number rises as the inlet temperature rises. Figure shows that the convergent divergent nozzle's Mach number is lower at 300K than it is at 1200K, where it reaches its maximum value.

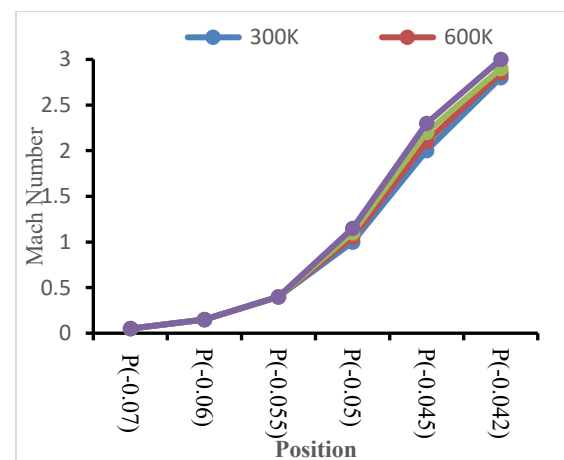


Figure 10: Mach Number Along Nozzle Length

#### IV. CONCLUSION

The present investigations compare the effect of different convergent angles of a supersonic nozzle to evaluate the thrust force; the computational code was validated with experimental data. The effect of various working fluids, such as air, CO, CO<sub>2</sub>, and N<sub>2</sub>, as well as the effect of inlet temperature on Mach number were studied.

The numerical simulation of a CD nozzle with various convergent angles yielded the following conclusions:

1. The convergent angle has a significant impact on thrust force. Moreover, based on the current design, the reduction in convergent angle has a positive effect on the thrust performance of the nozzle up to 27°, after which the thrust production of the nozzle decreases.
2. At a convergent angle of 27°, it was estimated that the thrust performance of the nozzle improved by 1.6% compared to its baseline design.
3. CO<sub>2</sub> has the highest thrust performance, followed by N<sub>2</sub>, air, and CO.
4. An increase in inlet temperature results in an increase in Mach and that there is a linear relationship between inlet temperature and Mach number.

#### REFERENCES

- [1] S. Baumann and U. Klingauf, "Modeling of aircraft fuel consumption using machine learning algorithms," *CEAS Aeronaut. J.*, vol. 11, no. 1, pp. 277–287, 2020, doi: 10.1007/s13272-019-00422-0.
- [2] J. J. Sangiovanni, T. J. Barber, and S. A. Syed, "Role of hydrogen/air chemistry in nozzle performance for a hypersonic propulsion system," *J. Propuls. Power*, vol. 9, no. 1, pp. 134–138, 1993, doi: 10.2514/3.11495.
- [3] S. M. V. Rao and G. Jagadeesh, "Novel supersonic nozzles for mixing enhancement in supersonic ejectors," *Appl. Therm. Eng.*, vol. 71, no. 1, pp. 62–71, 2014, doi: 10.1016/j.applthermaleng.2014.06.025.
- [4] I. MIR, S. SAMO, T. HUSSAIN, I. ALI, and H. A. K. DURANI, "Influence of Convergent Section Length and Angle on Performance of Supersonic Nozzle," *Sindh Univ. Res. J. - Science Ser.*, vol. 49, no. 004, pp. 727--732, 2017, doi: 10.26692/surj/2017.12.48.
- [5] P. Biju Kuttan and M. Sajesh, "Optimization of divergent angle of a rocket engine nozzle using Computational Fluid Dynamics," *Int. J. Eng. Sci.*, no. 1, pp. 196–207, 2013.
- [6] A. F. El-Sayed, "Turbine-Based Engines: Turbojet, Turbofan, and Turboramjet Engines," *Fundam. Aircr. Rocket Propuls.*, pp. 403–529, 2016, doi: 10.1007/978-1-4471-6796-9\_6.
- [7] A. Royne and C. J. Dey, "Effect of nozzle geometry on pressure drop and heat transfer in submerged jet arrays," *Int. J. Heat Mass Transf.*, vol. 49, no. 3–4, pp. 800–804, 2006, doi: 10.1016/j.ijheatmasstransfer.2005.11.014.
- [8] I. M. Chohan, A. Ahmad, N. Sallih, N. Bheel, M. Ali, and A. F. Deifalla, "A review on life cycle assessment of different pipeline materials," *Results Eng.*, vol. 19, 2023, doi: 10.1016/j.rineng.2023.101325.
- [9] A. Bruccoleri, R. Leiter, M. Drela, and P. Lozano, "Experimental Effects of Nozzle Geometry on Flow Efficiency at Low Reynolds Numbers," *J. Propuls. Power*, vol. 28, no. 1, pp. 96–105, 2012, doi: 10.2514/1.56728.
- [10] R. L. Bayt and K. S. Breuer, "Viscous effects in supersonic MEMS-fabricated micronozzles," *Am. Soc. Mech. Eng. Dyn. Syst. Control Div. DSC*, vol. 66, pp. 117–123, 1998.
- [11] N. M. Khattab and M. H. Barakat, "03/02551 Modeling the design and performance characteristics of solar steam-jet cooling for comfort air conditioning Khattab, N. M. and Barakat, M. H. Solar Energy, 2002, 73, (4), 257–267," *Fuel Energy Abstr.*, vol. 44, no. 6, p. 408, 2003, [Online]. Available: <http://linkinghub.elsevier.com/retrieve/pii/S0140670103926804>
- [12] A. Balabel, A. M. Hegab, M. Nasr, and S. M. El-Behery, "Assessment of turbulence modeling for gas flow in two-dimensional convergent-divergent rocket nozzle," *Appl. Math. Model.*, vol. 35, no. 7, pp. 3408–3422, 2011, doi: 10.1016/j.apm.2011.01.013.
- [13] V. Emelyanov, K. Volkov, and M. Yakovchuck, "Transverse Jet Injection into a Supersonic Nozzle Flow," *30th Int. Symp. Shock Waves 1*, pp. 77–81, 2017, doi: 10.1007/978-3-319-46213-4\_12.
- [14] E. Propulsion, "19th AIAA/DGLR/JSASS International Electric Propulsion," in *19th AIAA/DGLR/JSASS International Electric Propulsion Conference*, 1987.
- [15] A. D. Ketsdever, M. T. Clabough, S. F. Gimelshein, and A. Alexeenko, "Experimental and numerical determination of micropropulsion device efficiencies at low reynolds numbers," *AIAA J.*, vol. 43, no. 3, pp. 633–641, 2005, doi: 10.2514/1.10284.
- [16] M. V. Whalen, "Low Reynolds Number Nozzle Flow Study," *NASA Tech. Memo.*, 1987.
- [17] M. H. Mohd Noh, "Numerical Investigation of Choked Converging-Diverging Nozzles for Thruster Application," *IJUM Eng. J.*, vol.

- 12, no. 3, 2011, doi: 10.31436/iiumej.v12i3.67.
- [18] J. H. Kim, H. D. Kim, and T. Setoguchi, "The effect of diffuser angle on the discharge coefficient of a miniature critical nozzle," *J. Therm. Sci.*, vol. 19, no. 3, pp. 222–227, 2010, doi: 10.1007/s11630-010-0222-2.
- [19] H. Jia, Y. Jian, B. Yin, J. Yang, and Z. Liu, "Experimental study on the combustion, emissions and fuel consumption of elliptical nozzle diesel engine," *Energy*, vol. 262, 2023, doi: 10.1016/j.energy.2022.125449.
- [20] Z. Li, Q. Zhang, F. Zhang, H. Liang, and Y. Zhang, "Investigation of Effect of Nozzle Numbers on Diesel Engine Performance Operated at Plateau Environment," *Sustain.*, vol. 15, no. 11, 2023, doi: 10.3390/su15118561.
- [21] F. H. Reema, "Theoretical Aspects on Design and Performance Characteristics for Solid Rocket Motor," *Int. J. All Res. Educ. Sci. Methods*, vol. 10, no. 2, pp. 2455–6211, 2022.
- [22] H. A. Kutty and P. Rajendran, "3D CFD simulation and experimental validation of small APC slow flyer propeller blade," *Aerospace*, vol. 4, no. 1, 2017, doi: 10.3390/aerospace4010010.
- [23] I. M. Chohan, A. Ahmad, N. Bheel, T. Najeh, and A. H. Almaliki, "Sustainability assessment of different pipeline materials in freshwater supply systems," *Front. Mater.*, vol. 12, 2025, doi: 10.3389/fmats.2025.1566151.
- [24] I. Zbiciński and X. Li, "Conditions for accurate CFD modeling of spray-drying process," *Dry. Technol.*, vol. 24, no. 9, pp. 1109–1114, 2006, doi: 10.1080/0737930600778221.
- [25] A. Z. Dhunny, M. R. Lollchund, and S. D. D. V. Rughooputh, "Wind energy evaluation for a highly complex terrain using Computational Fluid Dynamics (CFD)," *Renew. Energy*, vol. 101, pp. 1–9, 2017, doi: 10.1016/j.renene.2016.08.032.
- [26] W. El-Askary and A. Balabel, "Prediction of reattachment turbulent shear flow in asymmetric divergent channel using linear and non-linear turbulence models, Eng," *Res. J. (ERJ), Fac. Eng., Menoufiya Uni*, vol. 30, no. 4, pp. 535–550, 2007.
- [27] K. Chattopadhyay, M. Isac, and R. I. L. Guthrie, "Physical and mathematical modelling of steelmaking tundish operations: A review of the last decade (1999-2009)," *ISIJ Int.*, vol. 50, no. 3, pp. 331–348, 2010, doi: 10.2355/isijinternational.50.331.
- [28] A. Balabel, "RANS Modeling of Gas Jet Impinging Onto a Deformable Liquid Interface," *Emirates J. Eng. Res.*, vol. 12, no. 3, pp. 35–46, 2007.
- [29] A. M. Hegab, A. A. Balabel, and S. El-behery, "RANS Simulation of Turbulence in a Porous Channel with Constant Mass RANS Simulation of Turbulence in a Porous Channel with Constant Mass Injection," no. December 2014.
- [30] I. M. Chohan, A. Ahmad, N. Sallih, N. Bheel, W. M. Salilew, and A. H. Almaliki, "Effect of seawater salinity, pH, and temperature on external corrosion behavior and microhardness of offshore oil and gas pipeline: RSM modelling and optimization," *Sci. Rep.*, vol. 14, no. 1, 2024, doi: 10.1038/s41598-024-67463-2.
- [31] J. P. Dussauge, P. Dupont, and J. F. Debiève, "Unsteadiness in shock wave boundary layer interactions with separation," *Aerosp. Sci. Technol.*, vol. 10, no. 2, pp. 85–91, 2006, doi: 10.1016/j.ast.2005.09.006.
- [32] K. PLOTKIN, "Shock wave oscillation driven by turbulent boundary-layer fluctuations," *AIAA J.*, 1973, doi: 10.2514/6.1973-662.
- [33] Y. Bartosiewicz, Z. Aidoun, P. Desevaux, and Y. Mercadier, "Numerical and experimental investigations on supersonic ejectors," *Int. J. Heat Fluid Flow*, vol. 26, no. 1, pp. 56–70, 2005, doi: 10.1016/j.ijheatfluidflow.2004.07.003.
- [34] "Hino, T., K. Suzuki, and Y. Takagi, Modification of k- $\omega$  turbulence model for ship resistance flow predictions. Journal of Ocean Engineering and Marine Energy, 2022. 8(4): p. 527-538."
- [35] H. Antti, "Some improvements in Menter's k- $\omega$  SST turbulence model," *29th AIAA, Fluid Dyn. Conf.*, 1998, [Online]. Available: <http://dx.doi.org/10.2514/6.1998-2554>
- [36] M. Linares, A. Ciampitti, and M. Robaina, "Design Optimization of a Supersonic Nozzle," p. 170, 2015.
- [37] "Inc., F., Fluent 6.3.2, User Guide. 2006."
- [38] A. J. Eder, C. F. Silva, M. Haeringer, J. Kuhlmann, and W. Polifke, "Incompressible versus compressible large eddy simulation for the identification of premixed flame dynamics," *Int. J. Spray Combust. Dyn.*, vol. 15, no. 1, pp. 16–32, 2023, doi: 10.1177/17568277231154204.